

Nonlinear Modeling of F/A-18E Noise Propagation

Kent L. Gee^{*}, Victor W. Sparrow[†], Thomas B. Gabrielson[‡], and Anthony A. Atchley[§]

The Pennsylvania State University, University Park, PA, 16802

An algorithm has been developed to study the nonlinear propagation of high-amplitude jet noise. The hybrid time-frequency domain algorithm employs a split-step solution to a Mendousse-Burgers equation that includes the effects of quadratic nonlinearity, atmospheric absorption and dispersion, and geometrical spreading. Spectral predictions generated using the algorithm are compared to recent F/A-18E engine run-up noise measurements made at afterburner and military thrust conditions at distances of 74 and 150 m from the engine nozzles. The agreement between the predicted and measured spectra is such that the results help confirm that energy transfer is occurring to higher frequencies. However, the differences between the model and the measurement raise important issues regarding some of the physical phenomena likely associated with the measurement but not accounted for in the model. Among these are the substantial multipath interference effects in the measured spectra and the finite extent of the aeroacoustic sources within the jet.

Nomenclature

A	= ray-tube area (m^2)
c_0	= equilibrium sound speed (m/s)
f	= frequency (Hz)
$f_{r,N}$	= nitrogen relaxation frequency (Hz)
$f_{r,O}$	= oxygen relaxation frequency (Hz)
N_s	= number of data points in waveform
P	= Fourier transform of pressure (Pa/Hz)
p	= time-domain pressure (Pa)
r	= range variable (m)
\bar{r}	= plane-wave local shock formation distance (m)
$\alpha_{r,N}$	= absorption coefficient due to nitrogen (Np/m)
$\alpha_{r,O}$	= absorption coefficient due to oxygen (Np/m)
α_{tv}	= thermoviscous absorption coefficient (Np/m)
β	= coefficient of nonlinearity in air, $(\gamma+1)/2$
γ	= ratio of specific heats in air
Δr	= range step size (m)
η	= step size control parameter
ρ_0	= ambient density (kg/m^3)
τ	= retarded time $\tau = t - (r - r_0)/c_0$ (s)
$\Psi(f)$	= frequency-domain absorption/dispersion operator
$\psi(\tau)$	= time-domain absorption/dispersion operator

^{*} Ph.D. Candidate, Grad. Prog. in Acoustics, Penn State Univ., 202 Applied Science Bldg., University Park, PA 16802, kentgee@psu.edu, Student Member AIAA.

[†] Associate Professor of Acoustics, Grad. Prog. in Acoustics, Penn State Univ., 316B Leonhard Bldg., University Park, PA 16802, Senior Member AIAA.

[‡] Senior Research Associate, Applied Research Lab, Penn State Univ., P.O. Box 30, State College, PA 16804.

[§] Professor of Acoustics and Chair, Grad. Prog. in Acoustics, Penn State Univ., 217 Applied Science Bldg., University Park, PA 16802, Member AIAA.

I. Introduction

ALTHOUGH evidence exists that nonlinearity influences the propagation of noise radiated from high speed jets¹-³, significant work remains in order to more fully understand and accurately predict the nonlinear evolution of the noise spectrum. In particular, analyses have indicated that the propagation of noise radiated from the F/A-18E Super Hornet is nonlinear^{4,5}, but spectral predictions based on existing nonlinear jet noise prediction methods^{6,7} fail to adequately calculate the measured propagation⁴, likely due to their being based on unjustifiable assumptions. A model proposed by Crighton and Basforth⁶ calculated the evolution of the power spectrum based on a truncated series expansion solution and a Gaussian source assumption. Morfey and Howell⁷ proposed a more sophisticated nonlinear model equation that also operated on the power spectrum, but which required an additional assumption that the propagation was quasi-Gaussian. This paper presents prediction results obtained using a different method, which is based on previous work by Anderson⁸ and Pestorius and Blackstock⁹. First, the propagation model equation and its numerical solution are described. After a brief summary of the ground engine run-up measurements, the comparisons are made between nonlinearly and linearly predicted and measured spectra. These results are followed by relevant discussion and conclusions.

II. A Nonlinear Propagation Model

A. Governing Equation

A parabolic nonlinear propagation model equation that has been used fairly extensively is sometimes referred to as the Mendousse-Burgers equation¹⁰. The Mendousse-Burgers equation is the simplest model that accounts for the combined effects of nonlinear and dissipative processes. In its most basic form, it treats the propagation of planar waves through a thermoviscous medium; however, further development has yielded formulations of the equation that incorporate geometrical spreading¹¹ and arbitrary absorption and dispersion¹². The particular equation used hereafter will be referred to as the generalized Mendousse-Burgers equation (GMBE), which may be written as

$$\frac{\partial p}{\partial r} = \frac{\beta}{2\rho_0 c_0^3} \frac{\partial p^2}{\partial \tau} + \psi(\tau) p - \frac{1}{2A} \frac{\partial A}{\partial r} p, \quad (1)$$

where the variables are as defined in the nomenclature. Equation (1) describes the evolution of a pressure waveform as a function of range in terms of the three terms on the right-hand side, which account for nonlinearity, complex absorption and dispersion, and geometrical spreading, respectively. In general, the operator $\psi(\tau)$ in the GMBE may be arbitrary; however, in this case it represents complex absorption in the atmosphere.

The absorption and dispersion of sound in air is caused by thermoviscous and relaxation processes; however, dispersion due to thermoviscosity is considered negligible. The definition of $\psi(\tau)$ must correctly account for these mechanisms in order to correctly model the propagation. Bass *et al.*¹³ have provided an understanding of the sound absorption mechanisms in air, whereas one treatment of dispersion has been developed by Pierce¹⁰. To summarize these results, the complex absorption operator may be conveniently expressed in the frequency domain (cf. Ref. 12) as

$$\Psi(f) = -(\alpha_{tv} + \alpha_{r,O} + \alpha_{r,N}) + j \left(\frac{\alpha_{r,O}}{f_{r,O}} + \frac{\alpha_{r,N}}{f_{r,N}} \right) f, \quad (2)$$

where the real part of Eq. (2) represents absorption and the imaginary part represents dispersion and the variables are as defined in the nomenclature.

B. Other Physical Effects

There are multiple phenomena that typically affect outdoor sound propagation that are not considered by the nonlinear propagation model. First, any ground or any other multipath effects are ignored—the propagation is considered free-field. Second, the atmosphere is assumed to be homogeneous; temperature gradients and other causes of stratification are ignored. Finally, the atmosphere is considered quiescent. The presence of these effects in the actual measurement can very well lead to significant differences between predicted and measured values; however, the model in its current state represents a look at the nonlinear portion of the propagation, without other, potentially competing influences.

C. Numerical Solution

The form of the GMBE in Eq. (1) indicates that the nonlinear evolution of a pressure waveform as a function of range may be simply treated as the sum of the contributing processes. For a sufficiently small range step, the small-signal and finite amplitude effects may be considered independent and a split-step solution employed. This split-step solution consists of separating the GMBE into two equations and numerically evaluating each over a given range step. These equations are

$$\frac{\partial p}{\partial r} = \frac{\beta}{2\rho_0 c_0^3} \frac{\partial p^2}{\partial \tau}, \quad (3)$$

and

$$\frac{\partial P(f)}{\partial r} = \Psi(f)P(f) - \frac{1}{2A} \frac{\partial A}{\partial r} P(f). \quad (4)$$

Equations (3) and (4) respectively represent the change in pressure as a function of range due to nonlinearity and small-signal effects, namely complex absorption and geometrical spreading. Equation (4) is shown in the frequency rather than time domain for the purposes of algorithm implementation, which is described subsequently. The advantage of utilizing a split-step solution to the GMBE is that Eqs. (3) and (4) both have analytical solutions. The solution to Eq. (3) is known as the Earnshaw solution, which may be implemented numerically¹⁴ as

$$\tau_{r+\Delta r} = \tau_r - \frac{\beta \Delta r p(\tau_r)}{\rho_0 c_0^3}. \quad (5)$$

Equation (5) calculates the change in arrival time over the range step Δr for each point on the pressure waveform, yielding earlier arrival times for positive pressures and later arrival times for negative pressures. The amplitude-dependent shift of arrival times accounts for the physical phenomenon of waveform steepening.

Equation (4), which describes the losses suffered as a consequence of ordinary linear propagation, has a familiar solution, which is implemented numerically for assumed spherical spreading as

$$P(r + \Delta r, f) = \frac{r}{r + \Delta r} e^{\Psi(f)\Delta r} P(r, f). \quad (6)$$

Together, Eqs. (5) and (6) form the basis for an algorithm to implement the split-step solution to the GMBE.

D. Algorithm Implementation

The present algorithm has its roots in the work of Pestorius and Blackstock⁹, who studied the propagation of finite-amplitude noise in a long tube, and Anderson⁸, who investigated spherically-spreading spark pulses. Pestorius and Blackstock devised a hybrid time-frequency domain propagation algorithm that treated nonlinear effects in the time domain and boundary-layer absorption and dispersion in the frequency domain. The fast Fourier transform (FFT) was used to alternate between the two domains as necessary and weak-shock theory was used to prevent the appearance of multi-valued waveforms. Anderson eliminated the need for weak-shock theory by using an adaptive propagation step size and relying on thermoviscous absorption to ensure a singly-valued waveform at each range step. Others have since included molecular relaxation effects in studies of the propagation of sonic booms and other transient waveforms¹⁵⁻¹⁷.

The implementation of the algorithm may be summarized in the following steps:

- 1) The pressure waveform is truncated to N_s points, where N_s is a power of two. While not necessarily required, this step decreases algorithm computation time by maximizing FFT calculation efficiency. For the results presented in this paper, N_s was equal to 524,288 (2^{19}).
- 2) The absorption and dispersion coefficients that form $\Psi(f)$ are calculated *a priori* because of the assumed atmospheric homogeneity. If atmospheric stratification were included, $\Psi(f)$ would be recalculated along the propagation path as necessary.

- 3) The step size, Δr , is chosen adaptively to be $\Delta r = \eta \bar{r}$, where \bar{r} is the shock-formation distance for a plane wave in a lossless medium based on the current waveform shape, given by

$$\bar{r} = \rho_0 c_0^3 / \beta (dp/dt)_{\max}, \quad (7)$$

and η is a constant less than one. The derivative, dp/dt , is estimated using a forward-difference approximation. Because of geometrical spreading and atmospheric absorption, in reality a true discontinuity will only occur at a greater distance than \bar{r} in Eq. (7), which ensures that the waveform is always singly-valued for each Δr , assuming that $\eta \leq 1$. The value of η is selected based on the criterion that Δr is sufficiently small that the various propagation effects are indeed independent. A solution convergence study resulted in the use of $\eta = 0.2$ to obtain the results in this investigation.

- 4) Equation (6) is applied to the waveform to nonlinearly distort the time scale.
- 5) The entire waveform is transformed to the frequency domain, yielding a two-sided pressure spectrum that is N_s points in length. Transformation of the entire waveform, rather than treating it as multiple ensembles and transforming each separately, helps to minimize spectral leakage.
- 6) If the current range, r , corresponds to an element of a user-defined distance array at which power spectral calculations are desired, then the PSD is calculated using a frequency-domain averaging method outlined by Bendat and Piersol¹⁸.
- 7) The complex absorption and geometrical spreading step shown in Eq. (9) is applied to the single-sided pressure spectrum obtained from 5); the result is folded about the $N_s/2+1$ point to yield the correct two-sided spectrum.
- 8) The pressure spectrum is transformed back to the time domain yielding the small-signal equivalent waveform at $r + \Delta r$.
- 9) The waveform resulting from 8) combined with the distorted time scale obtained from 4) is resampled via linear interpolation, which yields a distorted waveform sampled at equal time increments.

Steps 3)-9) are then repeated until the maximum desired propagation distance has been reached. The version of the code used to generate the results in this paper also performs a parallel free-field linear prediction, which simply consists of the elimination of steps 4) and 9).

III. Measurement Summary

The F/A-18E/F run-up measurements were conducted at NAVAIR Lakehurst, NJ during the evening of 15 April 2003. Recordings with both engines at military thrust (Mil) and with afterburners (AB) engaged were made with Sony TCD-D8 digital audio tape recorders sampling at 44.1 kHz. During the tests, the approximate ambient temperature and relative humidity were 20° C and 50%, and average wind speeds were relatively low, approximately 3 m/s at a height of 4.5 m. The monitored wind direction, as well as a temperature inversion measured near the ground just before the engine run-ups, implies that the atmosphere was likely somewhat downward refracting. Data were acquired at 18, 74, and 150 m from the engine nozzles along a radial line 135° from the forward direction, which was found to be approximately the peak directivity angle for the F/A-18E at high-thrust conditions. Calculated overall sound pressure levels (OASPL) for each of the conditions and measurement locations are given in Table 1. The 18 m data were acquired with a Brüel & Kjaer 4938 6.35-mm (1/4-in) condenser microphone flush-mounted in an aluminum plate baffle located horizontally on pavement. The 74 and 150 m data were acquired with handheld Endevco 8510C-15 piezoresistive pressure transducers located about 1.2 m above grassy ground.

Before moving on the results and discussion sections, an additional note regarding the measurement environment should be made. The terrain over which the measurements were made was fairly inhomogeneous, which when

coupled with atmospheric effects may have led to what are believed to be unusually significant and complex multipath effects in the power spectra. The model does not incorporate these effects, and therefore, comparisons between measured and nonlinearly are not expected to completely agree. Therefore, the purpose of the comparison is to demonstrate that the model yields physically plausible results that agree with overall trends in the data.

Table 1. Measured OASPL (in dB re 20 μ Pa.)

	18 m	74 m	150 m
AB	151	135	127
Mil	147	132	123

IV. Results and Discussion

A. Time-domain Results

It is worthwhile to briefly discuss the qualitative behavior of the propagation algorithm before discussing the measured versus predicted spectral comparisons. As finite-amplitude noise propagates, waveform steepening occurs, resulting in a transfer of energy from the peak-frequency region of the spectrum to higher frequencies. If competing process, such as geometrical spreading and atmospheric absorption are insufficient to prevent the formation of shocks, energy may also be transferred downward in the spectrum as a result of shock coalescence.

Shown in Fig. 1 is the same small segment of the 18 m AB waveform as a function of retarded time, τ , at 18 m, 74 m, and 150 m. During the course of linear propagation, the waveform undergoes spherical spreading and atmospheric losses, which may be seen in an overall decrease in waveform amplitude and a slight smoothing of the waveform as high-frequency content is attenuated. Relative to the linearly predicted waveform, however, the nonlinear prediction demonstrates significant waveform steepening between 18 and 74 m. The shocks evident in Fig. 1b persist out to 150 m (see Fig. 1c), although it appears that the slopes at some of the shock fronts have increased slightly. Also, the continual process of steepening, resultant energy transfer to higher frequencies, and absorption of that high frequency energy by the atmosphere, yields overall amplitudes that are less than predicted by linear theory. These behaviors are qualitatively consistent with nonlinear propagation theory. Finally, examination of Figs. 1a-1c shows that for this small waveform segment, the algorithm does not predict significant shock coalescence between 18-150 m; there is evidence of some minor coalescence as well-defined shocks are formed between 18 and 74 m, but the relative location these shocks is largely unchanged between 74 and 150 m.

B. Spectral Results: Propagation from 18 to 74 m

The recorded AB and Mil waveforms at 18 m were numerically propagated using the described algorithm from 18 m to 74 m. The predicted power spectral densities (PSD) from these calculations are shown in Fig. 2, along with the measured PSD at 74 m. Relative to the linear prediction, the nonlinear PSD shows a loss of energy in the peak-frequency region of the spectrum, approximately 3.5 dB for the AB case and 2.5 dB for the Mil case, and energy transfer to the high and low ends of the spectrum. The spectral roll-off from 1-10 kHz is essentially 6 dB/octave in both cases, corresponding to a f^{-2} power law that is indicative of shock formation¹⁹. The fact that the f^{-2} slope continues out to 10 kHz signifies that the predicted characteristic rise time of the waveform shocks at 74 m for both AB and Mil is less than 0.1 ms, which is consistent with the small AB waveform segment in Fig. 1b.

Before making a comparison of the nonlinear predictions with the measured AB and Mil PSD at 74 m, some brief comments regarding the measured spectra are merited. Evident in the 74 m measured spectra are several significant minima, which are very likely due to multipath interference and propagation over substantially inhomogeneous terrain. The occurrence of the first of these minima between approximately 300-800 Hz is problematic because it raises some question as to what is actually occurring in the peak frequency region of the spectrum. Relative to the predicted spectra from 18 m, there is an apparent shift downward of the peak frequency at 74 m for both the AB and Mil cases. It is perhaps significant that a similar spectral shift has been observed in laboratory scale-model measurements¹. In Ref. 4, it was hypothesized that the shift could possibly be due to shock coalescence. The results of the nonlinear prediction model largely negate that argument—while the nonlinearly predicted PSD does indicate some energy transfer to low frequencies, the predicted peak frequencies do not change between the nonlinear and linear models. This implies that the fundamental cause of the peak frequency shift is not due to nonlinearity, but is attributed to other causes. Some possible causes for the shift will be discussed in the concluding section of this paper.

Despite the obvious disagreement between the nonlinearly predicted and measured PSD below 1 kHz, which is very likely exacerbated by the previously discussed spectral minimum in that region, agreement above 1 kHz is substantially better, particularly for the Mil case. Although there are multiple spectral minima in the measured PSD at 74 m, the results of the nonlinear model appear to capture the spectral trends over much of the frequency range for both engine settings. However, the beginnings of an exponential roll-off in the measured PSD at around 7 kHz for both AB and Mil implies that the characteristic shock rise time in the measured waveforms at 74 m is greater than that predicted by the nonlinear model. One possible explanation for the difference is the likely presence of atmospheric turbulence in the actual propagation, which, on average, has been shown to increase rise times relative to nonturbulent propagation²⁰.

C. Spectral Results: Propagation from 18 to 150 m

Calculated spectra from the numerical propagation of the 18 m AB and Mil waveforms out to 150 m are shown in Fig. 3 along with the measured PSD. Again, the apparent peak frequency shift exists between the predicted and

measured spectra. However, at high frequencies, unlike the 74 m comparison, there is a significant offset between the measured and nonlinearly predicted spectra, on the order of 8 dB for AB and 6 dB for Mil power. The predicted spectral slopes do, in fact, follow fairly closely those of the measured spectra, especially for the Mil case where the predicted PSD begins to deviate noticeably from the f^{-2} behavior at about 4 kHz. The AB nonlinearly predicted PSD also begins to roll off before 10 kHz, but not as significantly, which is not unexpected because of its initially higher OASPL.

D. Spectral Results: Propagation from 74 to 150 m

Predictions at 150 m were also calculated using the 74 m waveforms. The comparisons with the measured spectra are shown in Fig. 4. For this case, there is no shift in peak frequencies—the predicted and measured peak frequencies correspond very well, although the predicted energy at low frequencies is higher than measured by about 3 dB for both engine settings. At high frequencies, the nonlinear predictions from 74 m much more closely approximate the measured 150 m spectra than do those made from 18 m; the offset in predicted versus measured level is much smaller. This may be largely due to the fact that the measured 74 m peak frequencies match those of the 150 m measurement and the 18 m peak frequencies do not; however, this is largely conjecture. As a final point, it is noteworthy that the difference between linear and nonlinear predictions is less between 74 and 150 m than it is between 18 and 74 m, which implies that as the propagating waveform is reduced in amplitude due to the combined effects of spreading, absorption, and nonlinearity, the propagation begins to appear more linear.

V. Discussion and Conclusion

Comparisons between F/A-18E Super Hornet AB and Mil power measurements and the results of a nonlinear prediction algorithm have been carried out. The comparisons show substantially better agreement than previous models that operate solely on the PSD and neglected phase information. The outcome demonstrates further evidence that the excess energy at high frequencies in the measured spectra at 74 and 150 m is the result of nonlinear energy transfer; however, the results also indicate there are many issues still to be resolved. The numerical solution of the GMBE treats the combined effects of nonlinearity, atmospheric absorption and dispersion, and geometrical spreading; therefore the discrepancies between predicted and measured spectra are most likely attributable to those phenomena not considered by the model equation, some of which are significant for these particular set of measurements.

First of all, the significant multipath effects in the 74 and 150 m measured spectra suggest that the free-field assumption is certainly violated in this case. Certainly, the results of this investigation suggest that future run-up measurements be conducted over flat, homogeneous terrain, so that the multipath effects may at the very least be better quantified. Furthermore, the meteorological measurements made throughout the tests are insufficient to fully understand the effects of atmospheric refraction and turbulence, both of which can significantly influence the measured spectral levels and are ignored by the model. Finally, the one-dimensional propagation model necessarily neglects the finite extent of the aeroacoustic sources within the jet, and instead treats the input waveform as a compact source.

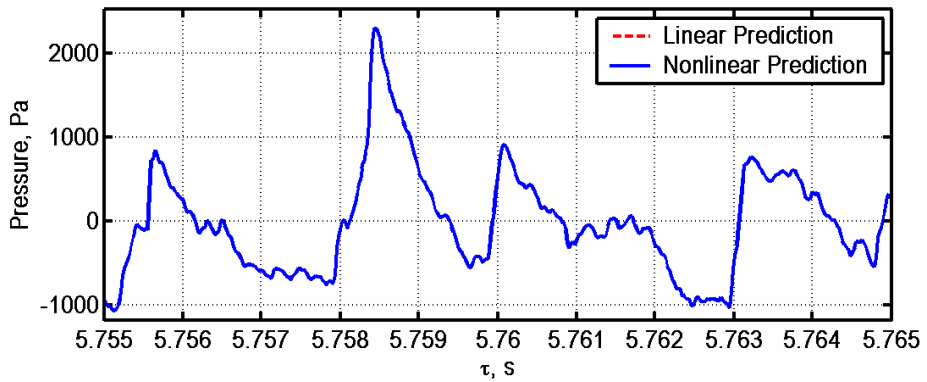
The possible problems created by the compact source simplification was considered by Blackstock³, but not resolved. At the present, the characteristics and extent of the acoustic near field of supersonic jets is largely unknown, and so it is also unknown at what points the propagation may be considered one-dimensional and the waveform spreading spherically. Koch *et al.*²¹ have showed that the origin of the geometric far field for subsonic jets is at a much greater distance for low frequencies than for high frequencies, due to the extended source distribution at low frequencies. It is possible that the apparent downward shift in peak frequency in Figs. 2 and 3 is partially caused by an assumption of spherical spreading in the both the linear and nonlinear predictions from 18 m and cylindrical-like spreading at low frequencies in the actual propagation. It is also possible that the apparent shift is related to the source directivity in that the effective propagation direction under the one-dimensional assumption is different for 18 m than it is for 74 or 150 m. It is likely that a number of factors, from near field effects to multipath interference, contribute to the apparent downward shift in peak frequency between the predicted and measured spectra in Figs. 2 and 3. The results of the propagation algorithm indicate, however, that the primary cause of the shift is not shock coalescence. Comparison of the nonlinear prediction model against additional data sets will increase understanding of the accuracy of the current model in reproducing actual jet noise propagation.

Acknowledgments

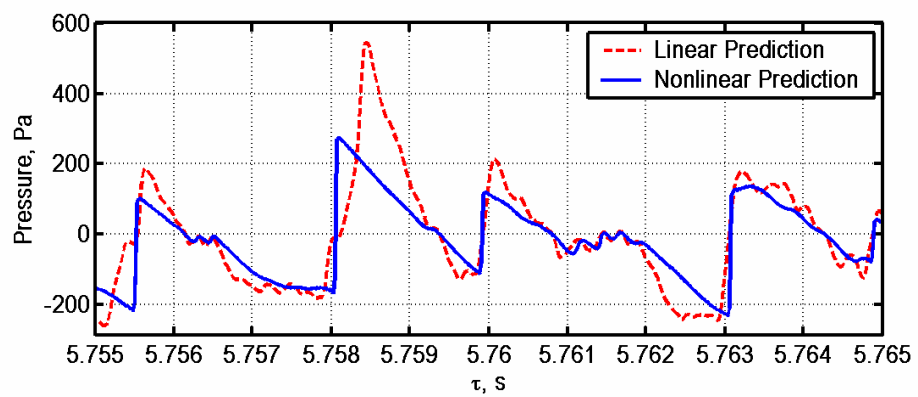
K. L. Gee and V. W. Sparrow are supported by the Strategic Environmental Research and Development Program, as a subcontract through Wyle Laboratories. A. A. Atchley and T. B. Gabrielson supported by the Office of Naval Research. The authors also gratefully acknowledge the cooperation of Richard McKinley and the Air Force Research Laboratory.

References

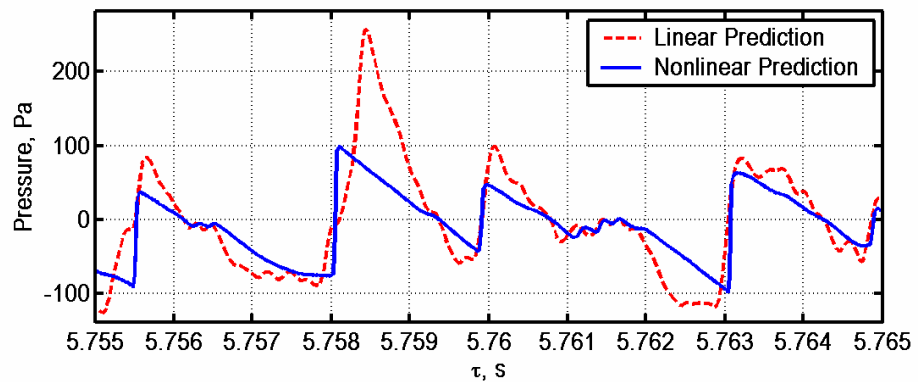
- ¹Gee, K. L., Petitjean, B. P., McLaughlin, D. K., and Sparrow, V. W., "Nonlinear Propagation of Noise Radiated from Supersonic Jets," *Proceedings of Noise-Con 04*, edited by C. B. Burroughs and G. C. Maling, Jr., Noise Control Foundation, Poughkeepsie, New York, 2004, pp. 725-733.
- ²Webster, D. A. and Blackstock, D. T., "Experimental Investigation of Outdoor Propagation of Finite-amplitude Noise," NASA CR-2992, 1978.
- ³Blackstock, D. T., "Nonlinear Propagation Distortion of Jet Noise," *Proceedings of the Third Interagency Symposium on University Research in Transportation Noise*, edited by G. Banerian and P. Kickinson, University of Utah, 1975, pp. 389-397.
- ⁴Gee, K. L., Gabrielson, T. B., Atchley, A. A., Sparrow, V. W., "Preliminary Analysis of Nonlinearity in F/A-18E/F Noise Propagation," AIAA paper 2004-3009, May 2004.
- ⁵Gee, K. L., Atchley, A. A., Falco, L. E., Gabrielson, T. B., and Sparrow, V. W., "Bispectral Analysis of High-Amplitude Jet Noise," AIAA paper 2005-2937, May 2005.
- ⁶Crighton, D. G., and Bashforth, S. "Nonlinear Propagation of Broadband Jet Noise," AIAA paper 80-1039, June 1980.
- ⁷Morfe, C. L. and Howell, G. P., "Nonlinear Propagation of Aircraft Noise in the Atmosphere," *AIAA Journal*, Vol. 19, No. 8, 1981, pp. 986-992.
- ⁸Anderson, M. O. "The Propagation of a Spherical N Wave in an Absorbing Medium and its Diffraction by a Circular Aperture," ARL TR 74-25 (AD787878), Univ. of Texas at Austin Applied Research Laboratories, Aug. 1974.
- ⁹Pestorius, F. M. and Blackstock, D. T. "Propagation of Finite-Amplitude Noise", *Finite-amplitude wave effects in fluids: Proceedings of the 1973 Symposium*, edited by L. Bjorno, IPC Business Press Ltd, Surrey, England, 1973, pp. 24-29.
- ¹⁰Pierce, A. D., *Acoustics: An Introduction to its Physical Principles and Applications*, Acoustical Society of America, Woodbury, NY, 1989.
- ¹¹Khokhlov, R. V., Naugol'nykh, K. A., and Soluyan, S. I. (1964), "Waves of moderate amplitudes in absorbing media," *Acustica*, Vol. 14, No. 5, pp. 241-247.
- ¹²Blackstock, D. T., "Generalized Burgers Equation for Plane Waves," *Journal of the Acoustical Society of America*, Vol. 77, No. 6, 1985, pp. 2050-2053.
- ¹³Bass, H. E., Sutherland, L. C., Zuckerwar, A. J., Blackstock, D. T., and Hester, D. M., "Atmospheric Absorption of Sound: Further Developments," *Journal of the Acoustical Society of America*, Vol. 97, No. 1, 1995, pp. 680-683 and "Erratum: Atmospheric Absorption of Sound: Further Developments," *Journal of the Acoustical Society of America*, Vol. 99, No. 2, 1996, p. 1259.
- ¹⁴Ginsberg, J. H. and Hamilton, M. F., "Computational Methods," Chap. 11 in *Nonlinear Acoustics*, edited by M. F. Hamilton and D. T. Blackstock, Academic Press, San Diego, CA, 1998.
- ¹⁵Orenstein, L. B., "The Rise Time of N Waves Produced by Sparks," ARL TR 82-51 (ADA120817), Univ. of Texas at Austin Applied Research Laboratories, Oct. 1982.
- ¹⁶Bass, H. E., Ezell, J. and Raspet, R. "Effect of vibrational relaxation rise times of shock waves in the atmosphere," *Journal of the Acoustical Society of America*, Vol. 74 , No. 5, 1983, pp. 1514-1517.
- ¹⁷Cleveland, R. O., Chambers, J. P., Bass, H. E., Raspet, R., Blackstock, D. T., and Hamilton, M. F., "Comparison of Computer Codes for the Propagation of Sonic Boom Waveforms through Isothermal Atmospheres," *Journal of the Acoustical Society of America*, Vol. 100, No. 5, 1996, pp. 3017-3027.
- ¹⁸Bendat, J. S., and Piersol, A. G., *Random Data: Analysis and Measurement Procedures*, 3rd ed., Wiley & Sons, New York, 2000, Chap. 11.
- ¹⁹Gurbatov, S. N. and Rudenko, O. V., "Statistical Phenomena," Chap. 13 in *Nonlinear Acoustics*, edited by M. F. Hamilton and D. T. Blackstock, Academic Press, San Diego, CA, 1998.
- ²⁰Blanc-Benon, P., Lipkens, B., Dallois, L., Hamilton, M. F., and Blackstock, D. T., "Propagation of finite amplitude sound through turbulence: Modeling with geometrical acoustics and the parabolic approximation," *Journal of the Acoustical Society of America*, Vol. 111, No. 1, 2002, pp. 487-498.
- ²¹Koch, L. D., Bridges, J., Brown, C., and Khavaran, A. "Numerical and Experimental Determination of the Geometric Far Field for Round Jets," NASA/TM—2003-212379, 2003.



a)

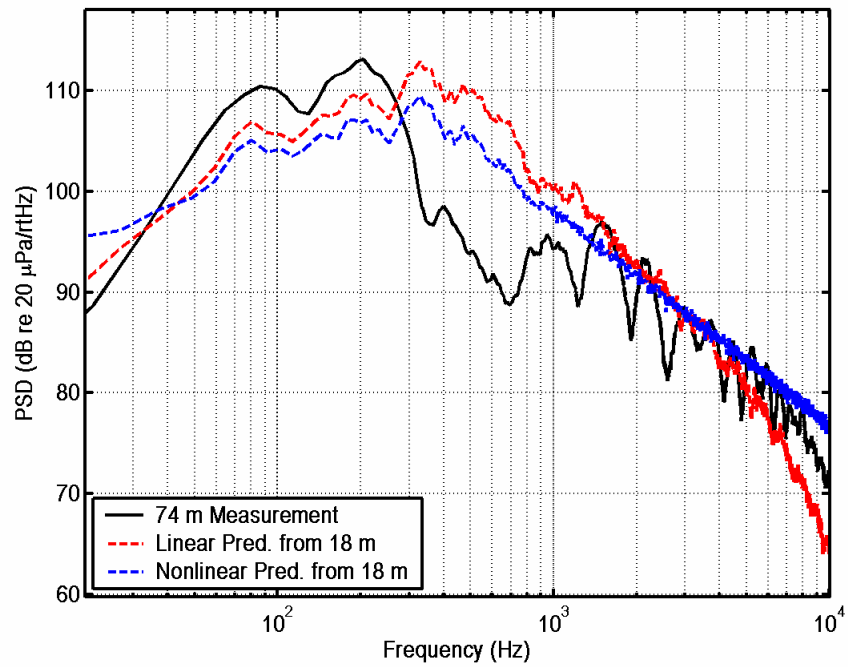


b)

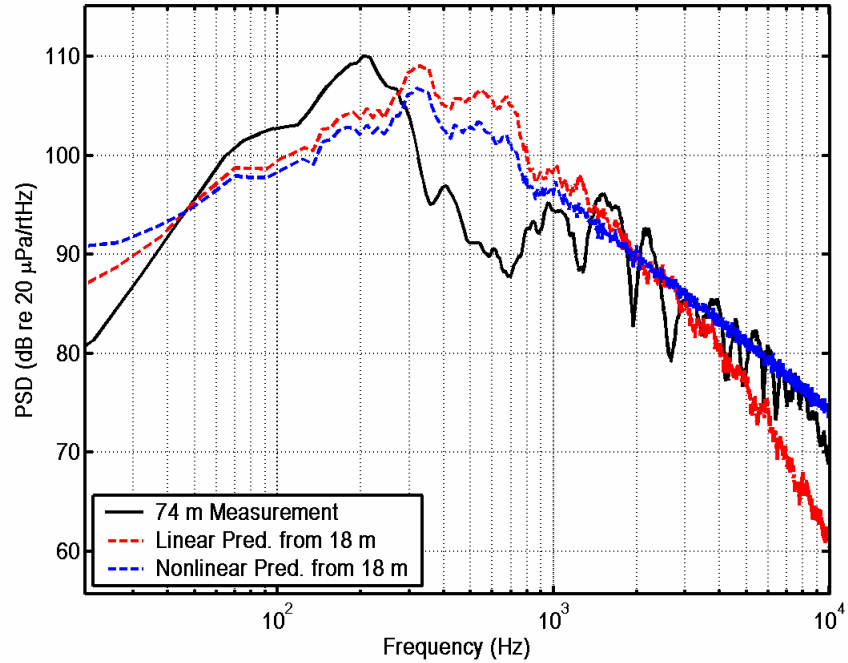


c)

Figure 1. AB waveform segment at a) 18 m, b) 74 m, and c) 150 m, showing linearly versus nonlinearly predicted waveforms. The linear and nonlinear predictions at 18 m exactly overlap because it is the algorithm reference distance.

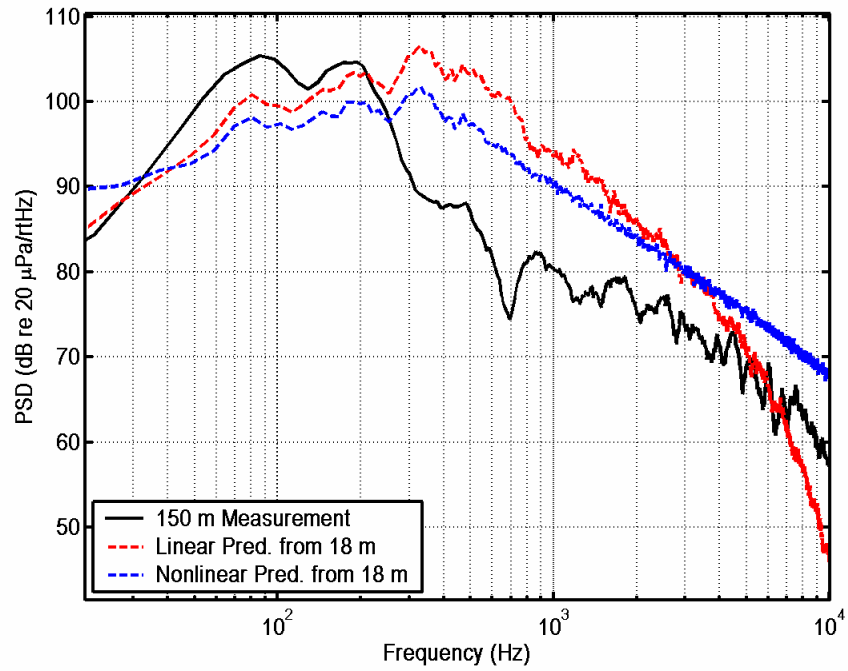


a)

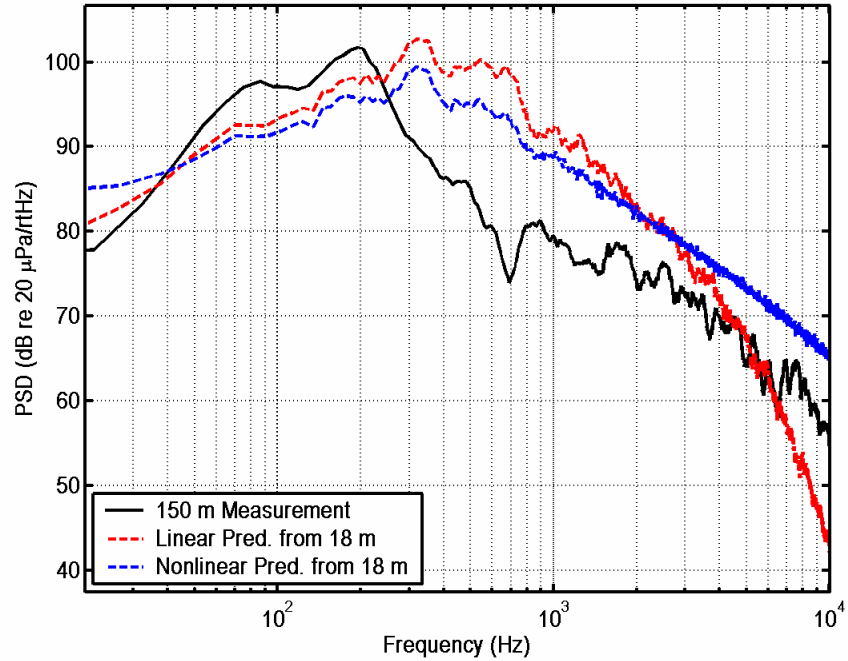


b)

Figure 2. Measured spectrum at 74 m versus linearly and nonlinearly predicted spectra from 18 m for a) AB and b) Mil.

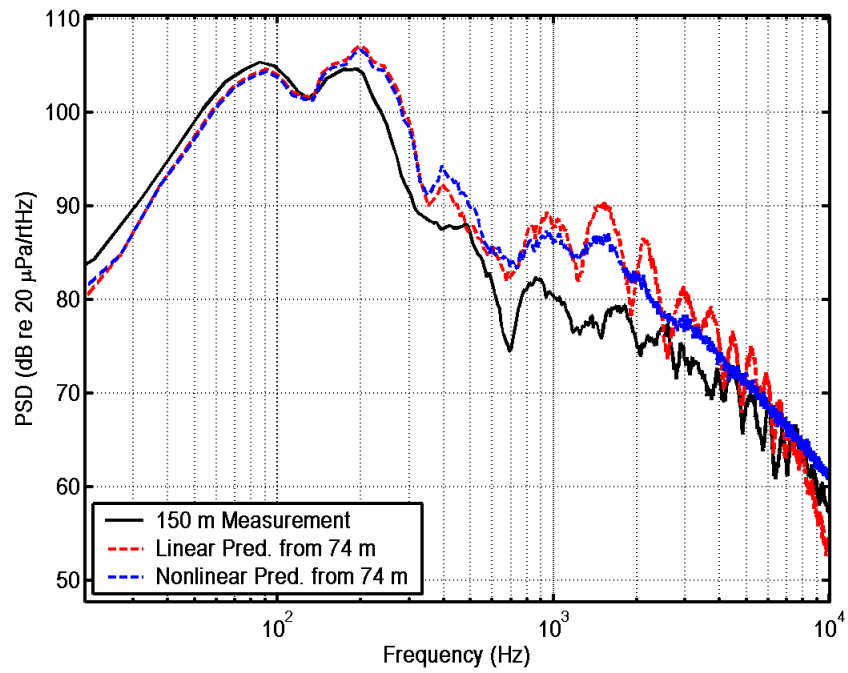


a)

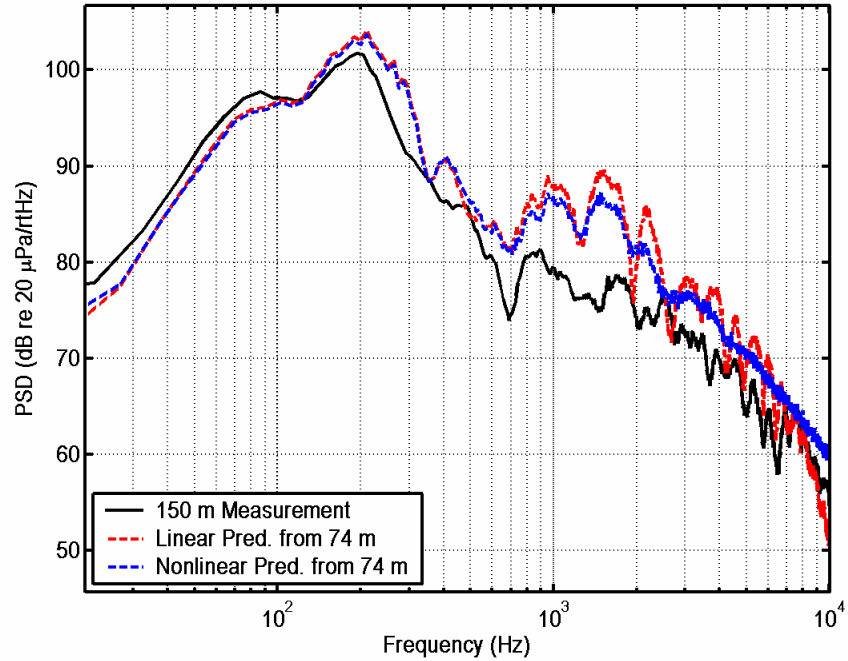


b)

Figure 3. Measured spectrum at 150 m versus linearly and nonlinearly predicted spectra from 18 m for a) AB and b) Mil.



a)



b)

Figure 4. Measured spectrum at 150 m versus linearly and nonlinearly predicted spectra from 74 m for a) AB and b) Mil.